Flow adjustment at the leading edge of a submerged aquatic canopy

WATER RESOURCES RESEARCH, VOL. 49, 5537–5551, doi:10.1002/wrcr.20403, 2013

Flow adjustment at the leading edge of a submerged aquatic canopy

Zhengbing Chen,[1,2] Chunbo Jiang,[1] and Heidi Nepf[2]

Received 21 March 2013; revised 2 July 2013; accepted 4 July 2013; published 10 September 2013.

[1] This paper describes the transition from open channel flow to flow over submerged vegetation using velocity measurements collected with acoustic Doppler velocimetry (ADV) and particle-image velocimetry (PIV). Submerged canopies were constructed from arrays of rigid circular cylinders of height h in water of depth H. Both the canopy density, described by the frontal area per volume (a), and degree of submergence (H/h) were varied. Flow adjustment occurs in three stages. First, velocity begins to decelerate upstream of the canopy, due to a high-pressure region generated at the canopy leading edge, and continues to decelerate within the canopy, due to canopy drag. Rapid flow deceleration within the canopy creates strong vertical flux out through the top of the canopy that extends over a length proportional to the canopy drag length scale, $(C_D a)^{-1}$, with C_D being the canopy drag coefficient. Second, a mixing layer develops at the canopy interface, with the stress at the top of the canopy initially increasing, but eventually reaching a constant value. At this point, the flow within the canopy is fully developed. The length scale for mixing-layer development is related to canopy drag ($C_D a$) and the depth ratio (H/h). In the third stage, the boundary layer above the mixing layer adjusts to the channel boundary conditions. A model is developed to predict the adjustment of vertically averaged velocity within the canopy. Measurements confirm that the flow adjustment is not dependent on canopy length.

Citation: Chen, Z., C. Jiang, and H. Nepf (2013), Flow adjustment at the leading edge of a submerged aquatic canopy, *Water Resour. Res.*, *49*, 5537–5551, doi:10.1002/wrcr.20403.

1. Introduction

[2] Aquatic vegetation plays a key role in many ecosystems [e.g., *Bunn and Arthington*, 2002]. It alters mean and turbulent flow, which in turn can influence the transport of sediment [e.g., *López and García*, 1998, 2001, *Nepf*, 2012]. The modified hydrodynamics can also impact nutrient uptake [*Morris et al*., 2008], light availability [*Madsen et al*., 2001], and metabolic function [*Nikora*, 2010]. The magnitude of flow through a canopy impacts the growth of organisms within the canopy. For example, reduced flow affects the food availability and growth of bivalves in a seagrass canopy [*Boström et al*., 2006].

[3] Most previous research has focused on fully developed flow over long canopies of vegetation (see review in *Nepf* [2012]). However, vegetation often grows in a mosaic of short patches [*Sand-Jensen and Madsen*, 1992], with individual patches too short to reach fully developed conditions. For typical river macrophytes, the distance to reach fully developed flow over a long canopy is 1–10 m [*Sukhodolov and Sukhodolova*, 2006; *Ghisalberti and Nepf*, 2009]. A few researchers have made observations of the transition in the mean and turbulent velocity at the leading edge of a canopy [*Gambi et al*., 1990; *Fonseca and Koehl*, 2006; *Kregting et al*., 2011; *Sukhodolova and Sukhodolov*, 2012], and these transition regions have been associated with higher nutrient uptake rates [*Morris et al*., 2008] and distinctive sediment deposition patterns [*Zong and Nepf*, 2010].

[4] Terrestrial vegetation has been studied more extensively than aquatic vegetation, with experimental and numerical methods describing flow adjustment at a forest edge [e.g., *Brunet et al*., 1994; *Irvine et al*., 1997; *Morse et al*., 2002; *Yang et al*., 2006; *Dupont et al*., 2011]. These studies introduce the following basic features of flow adjustment near a canopy leading edge (Figure 1). Let x and z be the streamwise and vertical directions, with velocity u and w, respectively. Overbar will denote time averages and prime will denote deviations from the time average, i.e., turbulent fluctuations.

[5] First, velocity begins to decelerate some distance upstream of the canopy, due to the high-pressure region generated at the canopy leading edge, and continues to decelerate within the canopy ($x > 0$), due to the canopy drag. From continuity, the deceleration of velocity within the canopy (U_c) is associated with a vertical velocity out from the canopy ($\overline{w} > 0$). The initial adjustment extends from the leading edge over length X_D (subscript D denotes deflection and deceleration). In this region, the mean vertical advection ($\overline{u}\,\overline{w}$) is significant relative to vertical turbulent transport ($\overline{u'w'}$) at the top of the canopy [*Yang et al*., 2006], and turbulence development is restricted by the

[1]State Key Laboratory of Hydro-Science and Engineering, Department of Hydraulic Engineering, Tsinghua University, Beijing, China.
[2]Department of Civil and Environmental Engineering, Massachusetts Institute of Technology, Cambridge, Massachusetts, USA.

Corresponding author: Z. Chen, State Key Laboratory of Hydro-Science and Engineering, Department of Hydraulic Engineering, Tsinghua University, Beijing 100084, China. (chenzb09@mails.tsinghua.edu.cn)

0043-1397/13/10.1002/wrcr.20403

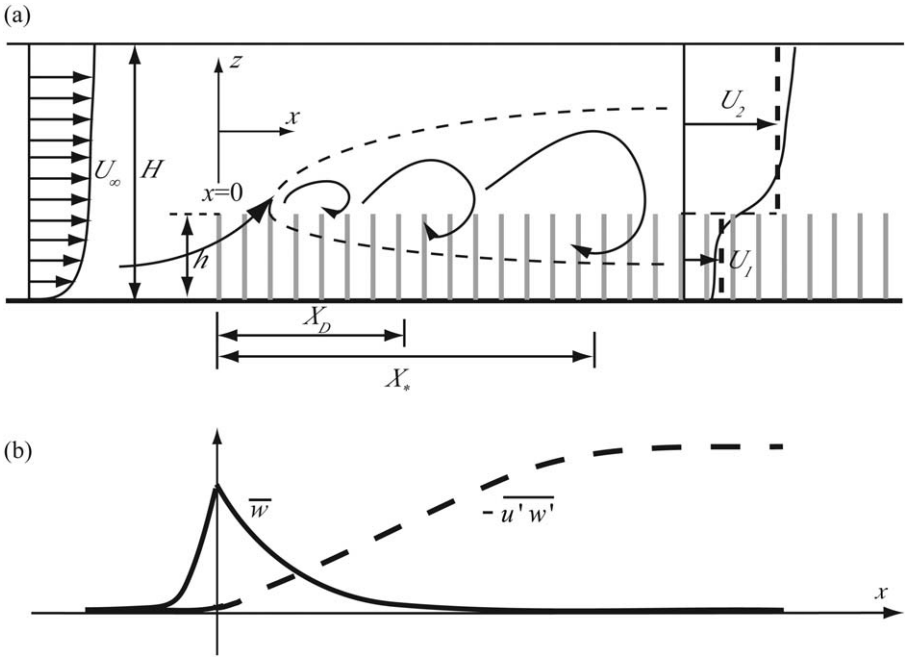

Figure 1. (a) Sketch of the flow adjustment from open channel flow to flow over submerged vegetation. H is the channel depth; h is the canopy height. X_D is the length of the initial adjustment, which corresponds to the deceleration of flow within the canopy. X_* is the length required for the mixing layer at canopy interface to reach its fully developed stage, at which point the friction velocity at the top of the canopy reaches a constant value, $u_* = \left(-\overline{u'w'}\right)_h^{1/2}$. Beyond X_*, U_1 is the vertically averaged flow within the canopy ($0 \le z \le h$), and U_2 is the vertically averaged flow above the canopy ($h \le z \le H$). (b) Longitudinal (x) profiles of time-mean vertical velocity ($\overline{w}$) and turbulent stress $\left(-\overline{u'w'}\right)$, both measured at the top of the canopy ($z = h$).

upward flow [*Irvine et al*., 1997; *Morse et al*., 2002]. Most terrestrial studies scale X_D with canopy height, h (typically 8–12 h), but acknowledge that X_D is dependent on the canopy density [e.g., *Yang et al*., 2006; *Dupont and Brunet*, 2009]. *Belcher et al*. [2003] suggest that X_D scales with the canopy drag length scale, L_c, which is a function of the frontal area per canopy volume (a), the canopy drag coefficient C_D, and the canopy solid volume fraction ϕ. Specifically, $L_c = 2(1-\phi)/C_D a$. Since most aquatic canopies have high porosity ($\phi < 0.1$), this may be approximated $L_c = 2/C_D a$.

[6] Second, a mixing layer with coherent vortex structures grows with distance from the leading edge, eventually reaching a fixed vertical size. As the layer grows, the turbulent stress at the top of the canopy ($-\overline{u'w'}$, Figure 1b) increases and eventually reaches a constant value at distance X_* from the leading edge. The subscript $_*$ connects this length scale to the maximum friction velocity at the top of the canopy, which we denote $u_* = \max\left(-\overline{u'w'}\right)_{z=h}^{1/2}$. Considering a forest canopy edge, *Irvine et al*. [1997] noted that all turbulence statistics eventually reach constant values in equilibrium with the canopy interface. This results in an equilibrium layer of finite height embedded within a boundary layer that continues to grow with distance from the leading edge. Unlike terrestrial flows, which are unbounded, aquatic flows are bounded by the water surface (Figure 1), so that the boundary layer can also reach a fully developed stage. In addition, small ratios of water depth (H) to canopy height (h) may impact flow adjustment. The objective of this paper is to describe the adjustment of flow from open channel conditions to vegetated flow, focusing on aquatic systems and the influence of water depth ratio (H/h). The following three questions will be addressed. What length scales describe the initial deceleration and mixing-layer growth? Does the initial flow adjustment depend on the canopy length? How much flow remains within the canopy layer?

2. Experimental Methods

[7] Experiments were conducted in a 16 m long, 1.2 m wide recirculating flume. The canopy was constructed with circular wooden dowels of diameter $d = 0.64$ cm. The dowels were held in a staggered pattern by a perforated baseboard. The array extended across the channel width, so that flow adjustment occurred only in the vertical plane. The canopy height was $h = 7$ cm above the baseboard. The frontal area per canopy volume is defined as $a = n_s d$, with n_s the number of dowels per unit bed area. Three canopy densities were tested; $a = 2.3$, 5.1, and 19.4 m^{-1}. Corresponding to these densities, three canopy lengths were used, $L = 4.8$, 3.0, and 1.5 m, respectively, chosen to ensure that the flow within the canopy reached full development, i.e., $L > X_*$. Because flow development was more rapid for denser canopies, we were able to make them shorter, which saved on labor and materials. For the medium density canopy, we added additional cases with $L < X_*$ (Table 1). The water depth was set by a downstream weir, and we targeted

Table 1. Parameters for Experiments[a]

Scenario	a (m^{-1})	L (m)	φ (%)	U_∞ (cm/s)	H (cm)	U_1 (cm/s)	U_2 (cm/s)	U_h (cm/s)	L_c (m)	X_w (cm)	X_D (m)	X_* (m)	u_* (cm/s)
A1	2.3	4.8	1.2	6.5	14.0	5.1	7.9	7.3	0.86	43 (11)	1.3 (0.3)	2.4 (0.3)	0.97
A2	2.3	4.8	1.2	5.9	27.7	3.0	6.9	4.5	0.86	59 (7)	1.8 (0.2)	1.9 (0.3)	0.81
A3	5.1	3.0	2.6	6.1	14.0	3.7	8.4	6.8	0.38	39 (6)	1.2 (0.2)	2.0 (0.2)	1.12
A4	5.1	3.0	2.6	6.3	21.8	2.8	8.0	5.2	0.38	38 (5)	1.1 (0.2)	1.8 (0.2)	1.05
A5	5.1	3.0	2.6	6.3	28.2	2.3	7.6	4.3	0.38	39 (2)	1.2 (0.1)	1.6 (0.2)	0.97
A6	19.4	1.5	9.8	6.2	14.0	1.5	11.0	7.0	0.06	17 (3)	0.5 (0.1)	1.1 (0.2)	1.20
A7	19.4	1.5	9.8	6.3	22.3	0.8	8.8	4.6	0.06	16 (2)	0.5 (0.1)	1.0 (0.2)	1.10
A8	19.4	1.5	9.8	6.4	27.6	0.7	8.3	3.8	0.06	19 (1)	0.6 (0.1)	1.1 (0.1)	1.00
B1	5.1	0.6	2.6	6.4	21.8								
B2	5.1	1.8	2.6	6.2	21.8								
B3	5.1	3.0	2.6	6.2	21.8								
	0.2	0.1	0.1	0.1	0.2	0.2	0.2						0.04

[a]For the A scenarios, the canopy length (L) is longer than X_*. For the B scenarios, the canopy length (L) is less than X_*, so U_1, U_2, X_w, X_D, X_*, u_* are not reported. X_w is the e-folding decay length for w, as discussed in section 4. u_* is the final, maximum friction velocity at the canopy interface ($z = h$). The last row provides the uncertainties for a, L, ϕ , U_∞, H, U_1, U_2, and u_*. Uncertainties in X_w, X_D, X_* are given in parentheses adjacent to the report value.

water depth ratios, $H/h = 2$, 3, and 4. The upstream velocity was set around $U_\infty = 6$ cm s^{-1}, but the specific values (Table 1) varied a bit with weir conditions. The range of water depths (14–28 cm), corresponded to depth-scale Reynolds numbers $Re_H = 8400$–16,800 and Froude numbers $Fr = 0.04$–0.05, indicating that the flow was fully turbulent and subcritical for all cases, so that no dependence on Re_H or Fr was expected. Drag coefficient C_D is determined from the cylinder Reynolds number, $Re_d = \overline{u}d/\nu$, evaluated at the leading edge, using relations provided in *Tanino and Nepf* [2008]. In general, C_D increases with increasing ϕ and decreasing Re_d. For the two smallest solid volume fractions (ϕ =1.2% and 2.6%), C_D is close to that of an isolated cylinder [*Tanino and Nepf*, 2008]. Using the empirical relation for an isolated cylinder, $C_D = 1 + 10Re_d^{-2/3}$, we estimate $C_D = 1.2$ [*White*, 1991]. For $\phi = 9.8\%$ ($a = 19.4$ m^{-1}), $C_D = 1.6$ from *Tanino and Nepf* [2008]. Experimental parameters are summarized in Table 1.

[8] The streamwise coordinate is x, with $x = 0$ at the leading edge of the canopy. The lateral coordinate is y, with $y = 0$ at the centerline of the flume. The vertical coordinate is z, with $z = 0$ at the bed. The three instantaneous components of velocity (u, v, w), corresponding to the streamwise, lateral and vertical coordinates, respectively, were measured with a Nortek *Vectrino* at a sampling rate of 25 Hz. Spikes in the velocity record were removed using the acceleration-threshold method [*Goring and Nikora*, 2002]. After despiking, each velocity record was decomposed into time-averaged ($\overline{u}, \overline{v}, \overline{w}$) and fluctuating components (u', v', w'), from which the turbulent intensities (u_{rms}, w_{rms}) and the Reynolds stress $\left(-\overline{u'w'}\right)$ were calculated.

[9] Flow inside a model canopy varies spatially at the scale of individual cylinders. This can be seen in the lateral profile of streamwise velocity taken at mid canopy height, $z = h/2$ (Figure 2). In this study, we are interested in the longitudinal evolution of velocity at scales larger than the heterogeneity associated with individual cylinders, and so we will only consider the spanwise-averaged velocity statistics, which we estimate using the following method. The spanwise average is shown in Figure 2 by a dashed line. We select from the lateral transect a measurement location (marked as cross in Figure 2) where the local velocity is close to the spanwise average. The measurement position, marked as cross, is also shown in the dowel array (Figure 2d). For the streamwise velocity, this method provides an estimate within 5% of the average. Figures 2b and 2c confirm that at the selected measurement location, the local values of vertical velocity (Figure 2b) and Reynolds stress (Figure 2c) are also representative, within 12% and 30%, respectively. The staggered array pattern repeats in the streamwise direction, so that we can use the same relative measurement position, as shown in Figure 2d, for each longitudinal measurement position. Because the array pattern varies with array density, this procedure was repeated for each density to identify the correct measurement position, which varies with array pattern. For the interested reader, we note that at the selected measurement point the lateral velocity and lateral flux do not reflect the spanwise average, which by definition are zero. However, this does not impact our analyses, which are restricted to spanwise average conditions

[10] Longitudinal transects of velocity began upstream of the canopy and extended to the end of the canopy. Depending on the canopy length and density, the spacing between measurement points was between 6 and 20 cm. For most cases, longitudinal transects were made at mid height ($z = h/2$) and at the top ($z = h$) of the canopy. Using the longitudinal transects as a guide, we selected locations for vertical profiles. For each measurement point, velocity was recorded for 4 or 6 min.

[11] Since vertical velocity was small, mostly less than 1 cm s^{-1}, acoustic streaming generated by the *Vectrino* acoustic pulses may affect the measurement of vertical velocity [*Poindexter et al*., 2011]. The acoustic streaming can range from negligible to more than 2 cm s^{-1}, depending on the *Vectrino* settings. In addition, if the probe is not aligned to vertical, streamwise velocity can be read as vertical velocity. In this case, the measured vertical velocity is correlated to the streamwise velocity, i.e., $\overline{w} = \overline{u}\sin\theta$, with θ the angular deviation of the probe axis from vertical. To evaluate probe alignment, we measured a vertical profile without model vegetation. We adjusted the vertical alignment until $\overline{w}(z)$ was not correlated to $\overline{u}(z)$, indicating that the probe was aligned. Once aligned, the depth-averaged vertical velocity should be zero. The measured depth-averaged vertical velocity was -0.2 cm s^{-1}, which was

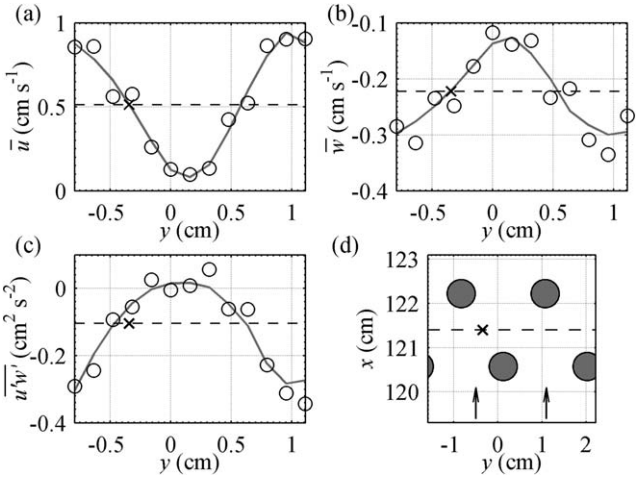

Figure 2. Lateral (y) profiles of time-averaged (a) streamwise velocity, (b) vertical velocity, and (c) Reynolds stress at midheight within the canopy ($z = h/2$) for case A7. The horizontal dashed lines indicate spanwise averages. The gray lines are smooth fits. (d) Dowel array. In each subplot, the measurement location is indicated by cross. The dash line in Figure 2d is the centerline between two rows.

consistent with the expected magnitude for acoustic streaming. Therefore, we concluded that acoustic streaming was present, contributing an offset of this magnitude to all vertical velocity measurements.

[12] Particle imaging velocimetry (PIV) was employed to confirm trends in flow evolution with higher spatial resolution. A Coherent Innova 70 Laser System was used to illuminate the flow. Polyamid seeding particles with a diameter of 50 μm (Dantec Inc.) were added to the water. A Dalsa Falcon HG camera was used to capture images. The camera has a resolution of 1400 by 1024 and maximum frame rate of 100 fps. For each measurement window (approximately 20 cm by 20 cm, shown in Figure 3) images were collected for 50 s at frame rates of 30–40 fps, which corresponds to 1500–2000 frames. The processing was performed with free software *PIVlab*. To improve image quality, the laser sheet wasn't placed on the centerline of the flume, but 30 cm away from centerline, closer to the glass side wall (Figure 3). To verify the PIV measurements, we compared PIV and *Vectrino* profiles measured in the channel without vegetation. The difference between the two profiles was less than 5%. Since the optimum measuring window was much smaller than the canopy length, a series of windows were measured along the canopy and joined together in postprocessing.

3. Results of PIV: An Overview of Flow Development

[13] Streamwise velocity, vertical velocity and Reynolds stress for scenario A7 (the most dense case) are shown in Figure 4. The patch began 3.5 m from the upstream end of the channel, which was not a sufficient distance to generate a fully developed boundary layer before the canopy. This is evident in the velocity profile upstream of the canopy, within which the velocity is 7 cm s^{-1} over most of the depth (yellow shading), decreasing toward the bed only for $z < 4$ cm. Approaching the canopy leading edge ($x = 0$), the flow begins to adjust first near the bed, with deceleration beginning 15 cm upstream of the canopy. *Belcher et al*. [2003] called this the upstream impact region. The deceleration upstream of the canopy is a response to the high-pressure zone created at the leading edge [e.g., *Yang et al*., 2006]. The length of the upstream impact region is comparable to the canopy height ($h = 7$ cm), which is consistent with previous studies of flow approaching porous layers [*Rominger and Nepf*, 2011; *Chen et al*., 2012]. As the velocity decreases near the bed, it must increase above the canopy, and continuity dictates a local region of high vertical velocity near the leading edge (Figure 4b). The maximum vertical velocity ($\overline{w} = 1.5$ cm s^{-1}) occurs at the leading edge ($x = 0$), after which it decays with distance, returning to zero at about $x = 40$ cm. Beyond this point ($x > 40$ cm), the streamwise velocity at the top of the canopy is constant with streamwise distance, x ($U_h = 0.05$ m s^{-1}, dark green), but the sheared region above the canopy continues to expand until it reaches the water surface. This reflects the sequential evolution of the mixing layer at the top of the canopy followed by the evolution of the boundary layer above the mixing layer. This progression is further illustrated by the evolution of the Reynolds stress.

[14] Along the top of the canopy, the Reynolds stress (Figure 4c) increases slightly directly at the leading edge, but then remain constant until $x = 40$ cm (blue region), which corresponds to the end of the region with strong vertical velocity (Figure 4b). As previously noted by *Morse et al*. [2002] and *Belcher et al*. [2003], the region of strong

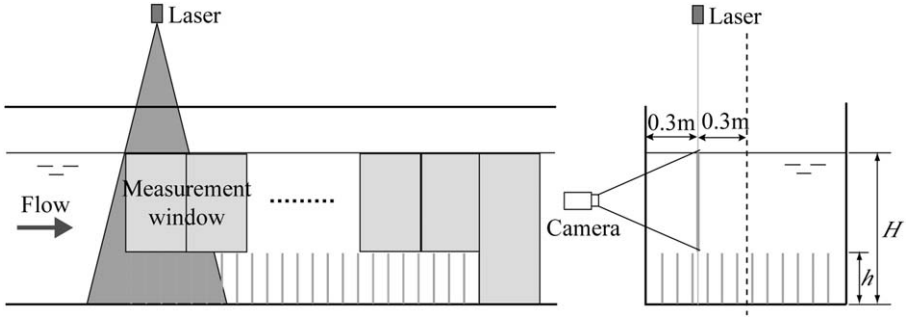

Figure 3. Sketch of laser and camera setup. The vertical coordinate is exaggerated. (left) A side view of the channel with the placement of PIV measurement windows. (right) The channel with flow into the page. The model canopy has height h in water depth H.

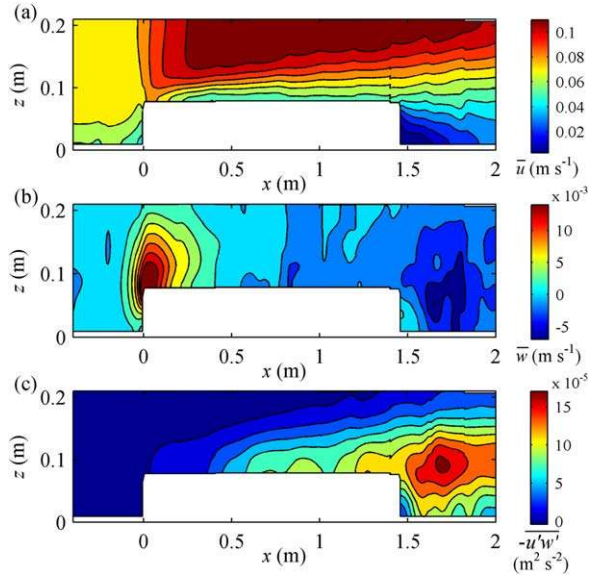

Figure 4. PIV contour plots of (a) streamwise velocity, (b) vertical velocity, and (c) Reynolds stress $-\overline{u'w'}$ for the most dense canopy, case A7 ($a = 19.4$ m^{-1}, $h = 7.0$ cm, $H = 22.3$ cm). The contours are evenly spaced with the intervals 0.01 m/s, 0.002 m/s and 0.2 × 10^{-4}m^2/s^2 for streamwise velocity, vertical velocity, and Reynolds stress, respectively.

vertical velocity at the leading edge interferes with the initial development of the canopy shear layer. Beyond $x = 40$ cm, the Reynolds stress increases linearly with x, until it levels to a value of 1×10^{-4} m^2 s^{-2} near $x = 1$ m, signaling the end of mixing-layer growth. As with the streamwise velocity, the profile of Reynolds stress above the canopy continues to develop until the boundary layer reaches the water surface.

[15] Although not the focus of this study, we note that in the wake of the canopy ($x > 1.5$ m) the velocity remains diminished to the end of the measurement region, which is 50 cm ($7h$) from the canopy trailing edge. Although not visible in the contour plot, a recirculation (negative local velocity) occurs at 10 cm (or about one canopy height) behind the trailing edge of the canopy. A peak in Reynolds stress occurs behind and slightly above the top of the canopy ($x = 1.7$ cm, $y = 10$ cm). These features have also been noted and discussed in previous studies of wakes behind model canopies [*Folkard*, 2005; *Detto et al*., 2008].

4. Initial Adjustment Region

[16] In the initial adjustment region, the streamwise velocity within the canopy decelerates, resulting (by continuity) in a vertical velocity at the top of the canopy, with a maximum vertical velocity at the leading edge (Figure 4b). Previous researchers have shown that the streamwise velocity decays exponentially within the canopy [*Lee*, 2000; *Belcher et al*., 2003], from which continuity dictates that the vertical velocity also decays exponentially, as we see in Figure 5. We use the following procedure to estimate the development length, X_D, from the longitudinal transects of vertical velocity measured at $z = h$ (Figure 5). Let $\overline{w}_s$ be the acoustic streaming offset, discussed in the methods section, and let $\overline{w}_0$ be the value at the leading edge ($x = 0$). The evolution of vertical velocity in x will have the following form (e.g., solid line in Figure 5)

$$\overline{w}(x) = \overline{w}_s + (\overline{w}_0 - \overline{w}_s)\, exp(-x/X_w) \tag{1}$$

in which X_w is the e-folding decay length for $\overline{w}$. For each canopy condition, X_w and its 95% confidence limit are extracted from (1) using a linear regression of x versus $ln[(\overline{w} - \overline{w}_s)/(\overline{w}_0 - \overline{w}_s)]$ (Table 1). A y intercept of zero is statistically supported ($p \gg 0.05$) for all cases, except A3 ($p = 0.02$). We define X_D at the point of 95% decay in $\overline{w}$, i.e., $X_D = 3X_w$.

[17] In Table 1, we see that X_w decreases as a increases. This is consistent with previous studies [*Belcher et al*., 2003; *Rominger and Nepf*, 2011] that correlated the length scale for flow adjustment to the drag length-scale $L_c \sim a^{-1}$. However, the scaling is not linear. Specifically, for our three canopy densities ($a = 2.3$, 5.1, and 19.4 m^{-1}) the scale factor increases with canopy density, $X_D = 2.1L_c$, $3.6L_c$, $9L_c$, respectively. *Coceal and Belcher* [2004] performed several numerical experiments to simulate the adjustment of a logarithmic wind profile to an urban canopy, varying the canopy density. From these experiments and a scale analysis, they proposed,

$$X_D = 3L_c \ln K \tag{2}$$

with $K = (U_h/u_*)(h/L_c)$. U_h is the streamwise velocity and u_* is the friction velocity, both at the top of canopy. For forest canopies, the factor 3 ln K is typically in the range 4.5–6 [*Belcher et al*., 2012] and for urban canopies in the range 1.5–6 [*Coceal and Belcher*, 2004]. In general, the scale factor 3 ln K has a larger value for denser canopies, which is consistent with the trend observed in our study. However, for the aquatic canopies considered in this study, (2) returns a negative value for cases A1 and A2, because K is less than 1 in these cases. This suggests that we cannot adopt

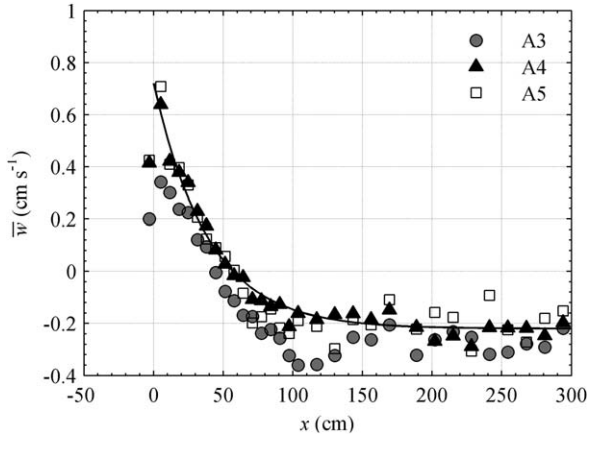

Figure 5. Vertical velocity ($\overline{w}$) along top of canopy ($z = h$) for cases A3, A4, and A5. For these three cases the depth ratio (H/h) is 2, 3, and 4, respectively, and the canopy density is $a = 5.1$ m^{-1}, $ah = 0.36$. The black line is equation (1) fitted for A4 (triangles).

the scaling defined in (2) for aquatic canopies. To gain insight into when the scaling breaks down, we explore the term $K = (U_h/u_*)\,(C_D a h(1-\phi)/2)$ appearing in (2). This parameter can be simplified with the following approximations. The velocity ratio U_h/u_* is fairly constant (3–6) across a wide range of canopy conditions [*Finnigan*, 2000; *Ghisalberti*, 2009], and in many aquatic canopies the factor $(1-\phi)$ is close to 1. With these simplifications $K = (1.5-3)\,C_D a h$. Because $K<1$ returns an invalid result in (2), we now see that (2) cannot be used for sparse canopies, specifically for $C_D a h \leq (0.3-0.7)$. Next, we propose a modification to the scaling that does not have this limitation.

[18] Consider the double-averaged momentum equation [e.g., *Wilson and Shaw*, 1977; *Nikora et al*., 2007].

$$\underbrace{\langle\overline{u}\rangle\frac{\partial\langle\overline{u}\rangle}{\partial x}}_{\text{(I)}}+\underbrace{\langle\overline{w}\rangle\frac{\partial\langle\overline{u}\rangle}{\partial z}}_{\text{(II)}}=\underbrace{-\frac{1}{n\rho}\frac{\partial n\langle\overline{p}\rangle}{\partial x}}_{\text{(III)}}\underbrace{-\frac{\partial n\langle\overline{u'w'}\rangle}{n\partial z}}_{\text{(IV)}}\underbrace{-\frac{1}{2n}C_D a\langle\overline{u}\rangle^2}_{\text{(V)}} \tag{3}$$

The overbar indicates a time average that removes temporal fluctuations at turbulent time scales. The bracket indicates a spatial average that removes the stem-scale heterogeneity within the canopy. The spatial average excludes the volume occupied by the canopy elements, which introduces the canopy porosity, $n = 1-\phi$. Because we only consider canopies of sufficient density to produce mixing layers ($ah \geq 0.1$, e.g., *Nepf* [2012, and references therein]), the dispersive stresses resulting from the spatial variation of time-averaged velocity are neglected. *Poggi et al*. [2004a] showed that for dense canopies ($ah \geq 0.13$) the dispersive stress is less than 10% of the Reynolds stress. We assume that the model canopy, like the canopy in our experiment, is spatially uniform, and specifically $n \neq \mathrm{f}(x, z)$, so that porosity is only important in the drag term.

[19] From (3), we see that the adjustment of velocity in the streamwise direction (term I) depends on: the mean vertical advection of streamwise momentum (term II); the pressure gradient (term III); the Reynolds stress gradient (term IV); and the canopy drag (term V). Previous studies considered a reduced form of (3) that included only the deceleration (term I) and canopy drag (term V), from which one expects $X_D \sim L_C \approx 2(1-\phi)(C_D a)^{-1}$ [e.g., *Belcher et al*., 2003]. However, *Yang et al*. [2006] showed that the pressure gradient and the vertical advection are both significant near the leading edge. Therefore, we retain these terms in the analysis of the adjustment length. However, we drop the Reynolds stress term, which is observed to be small near the leading edge (see discussion of Figure 1 above, and *Belcher et al*. [2003]). The following characteristic variables are used to scale (3),

$$\langle\overline{u}\rangle \sim U_\infty \tag{4}$$

where U_∞ is the upstream velocity.

$$x \sim X_D \tag{5}$$

From continuity,

$$\langle\overline{w}\rangle \sim U_\infty h/X_D. \tag{6}$$

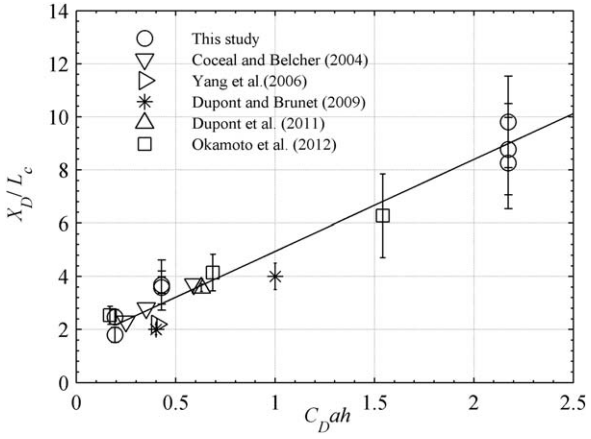

Figure 6. Initial adjustment length (X_D) normalized by canopy drag length scale (L_c) versus dimensionless canopy density, $C_D ah$. The solid line is the best fit of equation (9). The 95% confidence limits of the fit are $\alpha = 2.3 \pm 0.2$ and $\beta = 1.5 \pm 0.2$. Sources of individual data sets are discussed in the text.

Based on previous studies [*Rominger and Nepf*, 2011; *Belcher et al*., 2003], the elevation of pressure at the leading edge, Δp, increases with increasing canopy density (drag).

$$\frac{\Delta p}{\rho {U_\infty}^2} \sim C_D a h \tag{7}$$

[20] Substituting (4) through (7) into (3), and dropping the Reynolds stress, we get

$$-\frac{{U_\infty}^2}{X_D} \sim \frac{C_D a h {U_\infty}^2}{X_D} - \frac{1}{2(1-\phi)} C_D a {U_\infty}^2. \tag{8}$$

The following linear form satisfies the scale relation in equation (8)

$$\frac{X_D}{L_c} = \beta(1 + \alpha C_D a h) \tag{9}$$

with scale factors α and β to be determined from experimental data. Note that (9), unlike (2), directly reflects the contribution of pressure elevation at the leading edge, which leads to a nonlinear relationship between X_D and L_c.

[21] Data from five previous studies and measurements made in the present study support the relation proposed in (9) between X_D/L_c and $C_D ah$ (Figure 6). *Okamoto et al*. [2012] measured the velocity near the leading edge of a submerged canopy with PIV. In their experiment $h = 5$ cm, $U_\infty = 20$ cm s^{-1}, and the water depth was $H = 15$ cm ($H/h = 3$). The canopy densities were $a = 17.1$, 7.6, and 1.9 m^{-1}. The drag coefficient $C_D = 1.8$ was found in another discussion of the same experiments [*Nezu and Sanjou*, 2008]. We estimated X_D (0.4, 0.6, and 1.5 m, respectively) from streamwise profiles of vertical velocity [*Okamoto et al*., 2012, Figure 4]. *Coceal and Belcher* [2004] conducted numerical experiments of the adjustment of wind through model urban areas. The canopy height was 2.3 m,

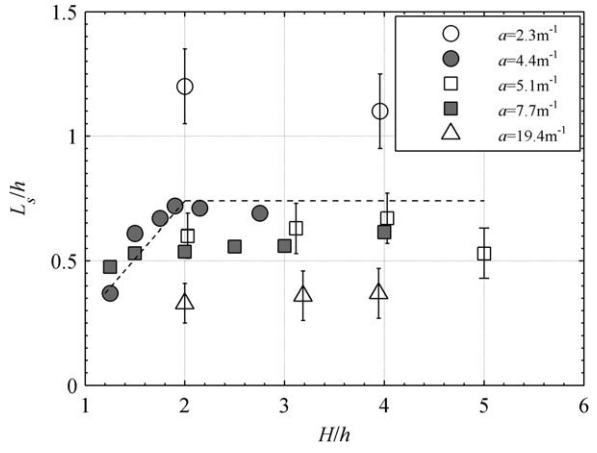

Figure 7. Variation of the shear length scale (L_s/h) with H/h and canopy density. *Nezu and Sanjou* [2008] (gray squares); *Nepf and Vivoni* [2000] (gray circles); the point ($a = 5.1$ m^{-1}, $H/h = 5$) is from D. Meire (unpublished data, 2012); other data from present study.

and the flow domain was nominally unbounded, i.e., H/h was effectively infinity. Three canopies were considered, with $L_c = 18.4$, 13.1, and 7.8 m, which corresponded to $X_D/L_c = 1.8$, 2.3, and 2.8, respectively. *Dupont and Brunet* [2009] simulated the flow development at the leading edge of a forest with height $h = 18$ m and drag coefficient $C_D = 0.2$. Two cases ($L_c = 90$ and 36 m) were considered, which resulted in adjustment lengths of $10h$ and $8h$, respectively. For the LES (Large Eddy Simulation) presented in *Yang et al*. [2006] ($h = 7.5$ m, $C_D = 0.2$, $a = 0.27$ m^{-1}) the vertical velocity at the top of the canopy went to zero at $X_D = (11 \pm 1)\ h$, from *Yang*'s Figure 6. Finally, *Dupont et al*. [2011] also considered a forest canopy ($h = 22$ m, $C_D = 0.26$). The canopy-average frontal area was $a = 0.11 \pm 0.01$ m^{-1} (Figure 2 of that paper). From *Dupont et al*. [2011, Figure 7], $\overline{w}_{z=h} = 0$ between 11 and $12h$, so $X_D = 250 \pm 10$ m. Data from the present study are summarized in Table 1. The solid line shown in Figure 6 represents the best fit of all data to equation (9), which yields, $\alpha = 2.3 \pm 0.2$ and $\beta = 1.5 \pm 0.2$.

$$\frac{X_D}{L_c} = 1.5(1 + 2.3 C_D a h) \tag{10}$$

[22] It is important to note that these data represent a wide range of submergence, $H/h = 2$ to effectively infinity (terrestrial cases), suggesting that X_D is not sensitive to submergence. This is seen explicitly in Table 1 for cases with $a = 5.1$ and 19.4 m^{-1}. Further, for the numerically modeled terrestrial canopies of *Yang et al*. [2006], *Dupont and Brunet* [2009], and *Dupont et al*. [2011], the frontal area of the canopy was a function of height, i.e., $a = f(z)$. For this analysis, however, we used the vertically averaged value of a, which is shown to produce good agreement with the trends of all data and with equation (10).

[23] Note that when $C_D a h >> 1$, equation (10) reduces to $X_D = 7(1 - \phi)h$. That is, X_D becomes predominantly a function of the canopy height, with the canopy density entering only through the porosity $(1 - \phi)$. This is similar to *Rominger and Nepf* [2011], who considered an aquatic canopy model that was uniform over flow depth (emergent), but of finite width (b = canopy half width). They found that for high flow blockage (large $C_D ab$), $X_D \sim b$, and specifically $X_D = 7b$. However, some caution is required when extrapolating (10) to large values of $C_D ah$, because the assumption that $\Delta p/\rho U_\infty{}^2$ increases linearly with $C_D ah$ (equation (7)), cannot extend indefinitely. As the canopy density approaches a solid body ($\phi = 1$), the pressure at the leading edge must asymptote to stagnation pressure, i.e., $\Delta p/\rho U_\infty{}^2 = 1$ (e.g., see Figure 6 in *Rominger and Nepf* [2011]), for which X_D is indeterminate in (8), but physics suggests X_D must approach zero.

5. Mixing-Layer Growth and Final Scale

[24] For canopies of sufficient density ($ah > 0.1$), flow at the top of a canopy resembles a mixing layer, rather than a boundary layer, although a boundary layer form is recovered at some distance above the canopy interface [e.g., *Raupach et al*., 1996; *Ghisalberti and Nepf*, 2002]. The mixing layer region is also known as the canopy-shear layer, equilibrium layer, or roughness sublayer. The canopy shear layer initially grows with distance from the leading edge, but the layer and the coherent structures it supports eventually reach a fixed size [*Ghisalberti and Nepf*, 2009] and a maximum contribution to vertical turbulent flux, which is manifest in a constant (with x) value of friction velocity, $u_* = \left(-\overline{u'w'}\right)^{1/2}$ defined at the top of the canopy (data discussed below). The distance from the canopy leading edge to the fully developed mixing layer is denoted as X_*. Below, we first discuss the vertical scale of the fully developed mixing layer, and then return to discuss its evolution from the leading edge.

[25] The scale of the fully developed mixing layer and the coherent structures it contains are determined by both the canopy density and the depth of submergence. The shear length scale, $L_s = U_h/(\partial < \overline{u} > /\partial z)_h$, is a measure of the coherent structure scale within the mixing layer [*Raupach et al*., 1996]. Note that this measure assumes that the shear at the top of the canopy is the maximum shear in the mixing layer, which has been observed to be true. *Nepf and Vivoni* [2000] suggested that the shear-length scale (L_s), as well as the penetration of coherent structures into the canopy, is constrained by the water surface if $H/h < 2$, and this limit was confirmed by *Wilson et al*. [2003]. Specifically, for a fixed canopy density (e.g., $a = 4.4$ m^{-1}, gray circles in Figure 7), L_s is constant for $H/h > 2$, but decreases with decreasing depth (H) for $H/h < 2$. A more recent study by *Nezu and Sanjou* [2008] suggests a smaller transition point ($H/h = 1.5$), which may indicate some dependence on canopy density (gray squares, Figure 7). *Ghisalberti* [2009] suggested that the water surface constrains the mixing layer when $C_D a(H - h) < 0.5$. Nevertheless, for all cases shown in Figure 7, L_s is not a function of H/h when $H/h > 2$, and this may be useful as a general limit.

[26] The shear length scale is a function of canopy density (a), with L_s/h decreasing as $C_D ah$ increases (Figure 8). For canopies with $C_D ah < 0.3$, the values $L_s/h > 1$ suggest that the mixing layer penetrates through the canopy height to the bed. This is consistent with the penetration scale, $\delta_e/h = [0.23 \pm 0.06]/(C_D ah)$, which describes the distance that

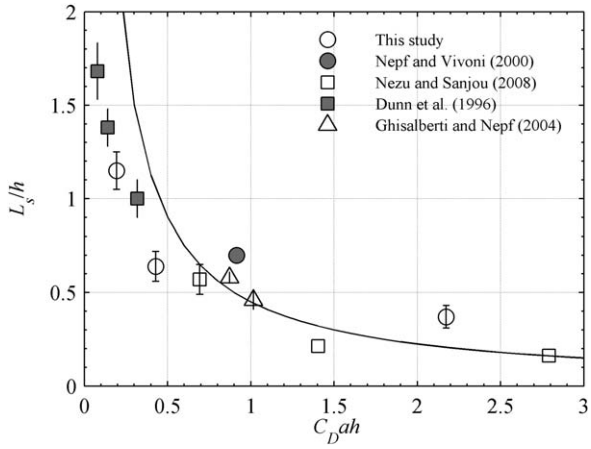

Figure 8. Shear-length scale normalized by canopy height, L_s/h, is inversely dependent on nondimensional canopy density, $C_D ah$. Data sources are given in legend. Only cases with $H/h \geq 2$ are included. The solid line correspond to curve $L_s/h = 0.4\,(C_D ah)^{-1}$.

the shear layer penetrates into the canopy, measured from the top of the canopy [*Nepf et al*., 2007]. That is, the coherent structures penetrate to the bed for $C_D ah < 0.23$. For denser canopies $C_D ah > 0.3$ (Figure 8) the mixing layer does not penetrate the full canopy height ($L_s/h < 1$).

[27] *Poggi et al*. [2004b] suggested the scaling $L_s \approx (2/C_D a)(u_*/U_h)^2$. However, the dependence on u_*/U_h is typically weak for canopies of sufficient density. Specifically, for $C_D ah > 0.3$, $(U_h - U_1) \approx 2.6u_*$ [*Ghisalberti*, 2009]. Further, for dense canopies, $U_1 << U_h$, indicating that u_*/U_h is roughly constant, suggesting the simplification $L_s/h \sim (C_D ah)^{-1}$. Fitting the data $C_D ah > 0.3$ produces the relation $L_s/h = 0.4\,(C_D ah)^{-1}$, shown as solid line in Figure 8.

[28] At some distance above the canopy, the velocity profile transitions from a mixing-layer type to a boundary layer type with a logarithmic form. *Poggi et al*. [2004b] suggest that the transition to an overlying log layer occurs

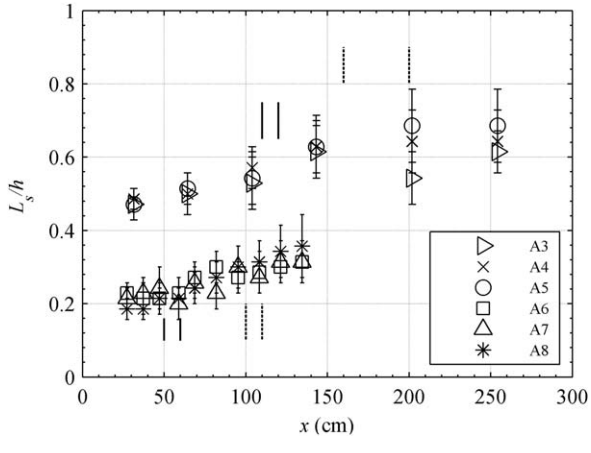

Figure 9. The normalized shear length scale, L_s/h, evolves from the leading edge of canopy. Canopy density $a = 5.1$ m^{-1} (A3, A4, A5, $ah = 0.36$) and 19.1 m^{-1} (A6, A7, A8, $ah = 1.3$). The vertical solid and dashed lines indicate X_D and X_*, respectively, for $a = 5.1$ m^{-1} and $a = 19.4$m^{-1}. See Table 1 for exact values.

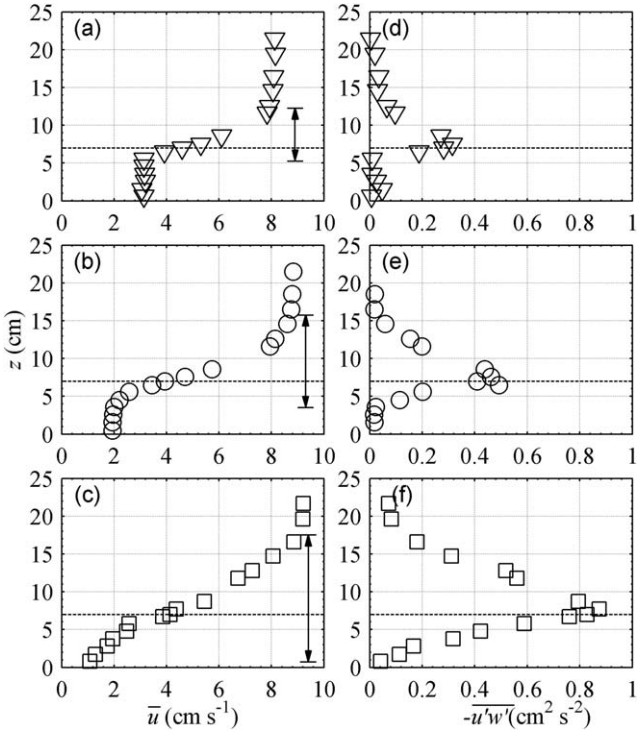

Figure 10. Evolution of streamwise velocity and Reynolds stress along the canopy for A5 ($H = 28.2$ cm, $a = 5.1$ m^{-1}). (a and d) $x = 30$ cm; (b and e) $x = 60$ cm; (c and f) $x = 140$ cm. Vertical scales shown in each graph depict the mixing layer thickness predicted from $\delta = 2(\Delta U/U_h)L_s$.

at $z = 2h$. Similarly, *Nezu* and *Sanjou* [2008, Figure 14 of that paper] estimated the transition occurred between $z/h = 1.65$ and 1.80, with no dependence on canopy density. Finally, assuming a mixing layer height of $2h$ produced a good fit to profiles measured over eelgrass in the field [*Lacy and Wyllie-Echeverria*, 2011].

[29] We now consider how the mixing layer develops from the leading edge of the canopy. The shear length-scale L_s/h increases with distance from the leading edge (Figure 9). The growth continues past the initial adjustment length X_D, but approaches a constant value around X_*, which will be discussed later. The progression of vertical profiles shown in Figure 10 gives more detail regarding the growth of the mixing layer. In a pure mixing layer, the physical thickness of the layer, δ, is twice the vorticity thickness $\left(\delta_w = \Delta U/(\partial\overline{u}/\partial z)_{\max}\right)$, with ΔU the velocity difference across the layer [*Pope*, 2000; *Sukhodolova and Sukhodolov*, 2012]. From these scales, we expect the mixing layer thickness to be $\delta = 2(\Delta U/U_h)L_s$, and this length scale is indicated alongside each profile in Figure 10. The lower limit of the mixing layer is taken at the point where the Reynolds stress decays to zero, within uncertainty. At $x = 140$ cm, the mixing layer has just touched the bed. Note that the mixing layer is not symmetric around the canopy interface, which has been noted previously [*Ghisalberti and Nepf*, 2002; *White and Nepf*, 2007]. In particular, *Ghisalberti and Nepf* [2002] found that the center of the mixing layer is positioned 0.5θ above the canopy interface, with θ the momentum thickness of the layer. The asymmetry is explained by the fact that once formed, the mixing-layer

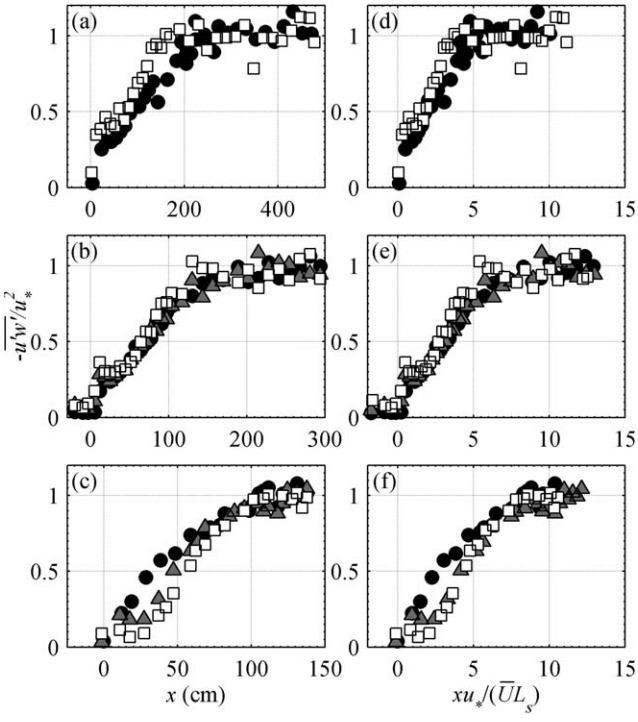

Figure 11. Reynolds stress at the top of the canopy, $-\overline{u'w'}_h$, normalized by the maximum value achieved (u_*) and shown (a–c) as a function of distance from the leading edge and also (d–f) as a function of the normalized distance. Three depths are considered: (filled circles) $H = 14$ cm; (solid triangles) $H = 22$ cm; (open squares) $H = 28$ cm. Three canopy densities are considered: (a and d) $a = 2.3$ m^{-1}; (b and e) $a = 5.1$ m^{-1}; (c and f) $a = 19.4$ m^{-1}.

coherent structures are influenced by the canopy drag, and they grow more away from the canopy than within it [*White and Nepf*, 2007]. Finally, in the field, *Sukhodolova and Sukhodolov* [2012] observed that δ grew linearly from the leading edge of a submerged meadow, which is consistent with Figure 10.

[30] The Reynolds stress at the top of the canopy $\left(-\overline{u'w'}_h\right)$ is an indicator of turbulent momentum exchange between the canopy and overflow. As the mixing layer evolves from the leading edge, $-\overline{u'w'}_h$ increases, but reaches a final, maximum value, u_*, once the mixing layer is fully developed (Figure 11). In some cases, the stress holds a nearly constant value for some distance at the leading edge, before beginning to increase. This is most evident for the densest canopy (Figure 11c, squares and triangles), for which the stress does not begin to increases until 40 cm past the leading edge (also shown in Figure 4c). Similarly, for $a = 5.1$ m^{-1} (Figure 11b), the constant stress near the leading edge extends to 50 cm. As mentioned above, this region of constant stress corresponds to the region of high vertical velocity, and the mixing layer only begins to develop after the vertical velocity becomes negligible compared to the friction velocity at the top of the canopy [e.g., *Belcher et al*., 2003].

[31] The mixing layer adjustment length (X_*) is the distance from the leading edge to the point at which the final, maximum Reynolds stress (u_*) is reached (Figure 11). This length scale has a clear inverse dependence on canopy density, with X_* increasing from 100 cm for the densest canopy ($a = 19.4$ m^{-1}) to 200 cm for the sparsest canopy ($a = 2.3$ m^{-1}) considered here (Figures 11a–11c and Table 1). For the densest canopy ($a = 19.4$ m^{-1}) X_* is the same within uncertainty for all depths of submergence (Table 1). However, for the other canopy densities, X_* is longer for conditions with shallower submergence (smaller H/h). As we discuss below, the dependence on submergence depth arises because the convective speed of the vortices within the mixing layer increases as H/h decreases.

[32] The following scaling argument is modified from *Ghisalberti and Nepf* [2009]. The mixing layer growth reflects the vertical diffusion achieved by the vortices in the layer, and we can define a time scale for this process (T_D) by taking L_s as a measure of the mixing layer thickness. We define a vertical diffusivity $D_z \sim u_* L_s$, based on observations and scaling given in *Ghisalberti and Nepf* [2005]. The time scale for mixing layer development is then,

$$T_D \approx \frac{{L_s}^2}{D_z} \sim \frac{L_s}{u_*}. \tag{11}$$

[33] The vortex convective velocity, U_v, translates this time scale into a length scale,

$$X_* \sim U_v T_d = \frac{U_v L_s}{u_*}. \tag{12}$$

[34] In a pure mixing layer, $U_v = \overline{U}$ [*Dimotakis et al*., 1981], which is the mean mixing layer velocity calculated from the lower (U_l) and upper (U_u) limits of velocity within the layer, i.e., $\overline{U} = (U_u + U_l)/2$. *Ghisalberti and Nepf* [2002] measured U_v in the mixing layer above a submerged canopy, and they found that $U_v/\overline{U} = 1.3 \pm 0.1$, with a weak dependence on depth of submergence, specifically, $U_v/\overline{U} = 0.93 + 0.12(H/h)$. For simplicity we use the scaling $U_v \sim \overline{U}$ in (12), from which we expect $X_* \sim \overline{U} L_s/u_*$. To evaluate this scaling, we normalized the coordinate x by $\overline{U} L_s/u_*$ in Figures 11d–11f. This collapses the different conditions, i.e., in each case the Reynolds stress reaches its maximum at the same normalized distance $X_* u_*/\overline{U} L_s = [8 \pm 2]$, which gives experimental support to the proposed scaling.

[35] We now consider the physical dependences embedded in $X_* \sim \overline{U} L_s/u_*$. This scaling suggests that X_* increases as canopy density (a) decreases, i.e., $X_* \sim L_s \sim a^{-1}$, which is consistent with our observations (Table 1). A dependence on submergence depth (H/h) emerges through $\overline{U}$, which is our surrogate for the vortex velocity U_v. $\overline{U}$ (and thus X_*) is inversely proportional to H/h (Table 1). This dependence arises directly from continuity. Consider an upstream flow with depth-averaged velocity U_∞. The flow in the canopy is decreased from this value by ΔU_1, i.e., $U_1 = U_\infty - \Delta U_1$. By continuity, the flow above the canopy must increase by $\Delta U_2 = (\Delta U_1 h)/(H - h)$, i.e., $U_2 = U_\infty + \Delta U_2$. From the constraints of continuity, $\overline{U} = {}^1\!/_2 (U_1 + U_2)$ can be written $\overline{U} = U_\infty + {}^1\!/_2 \Delta U_1 ((h/H - h) - 1)$. Since ΔU_1 is predominantly a function of a and not H/h, and letting h be constant for a fixed canopy, we see from this relation that as H (and thus H/h) decreases, $\overline{U}$ (and thus X_*) increases. Since this constraint

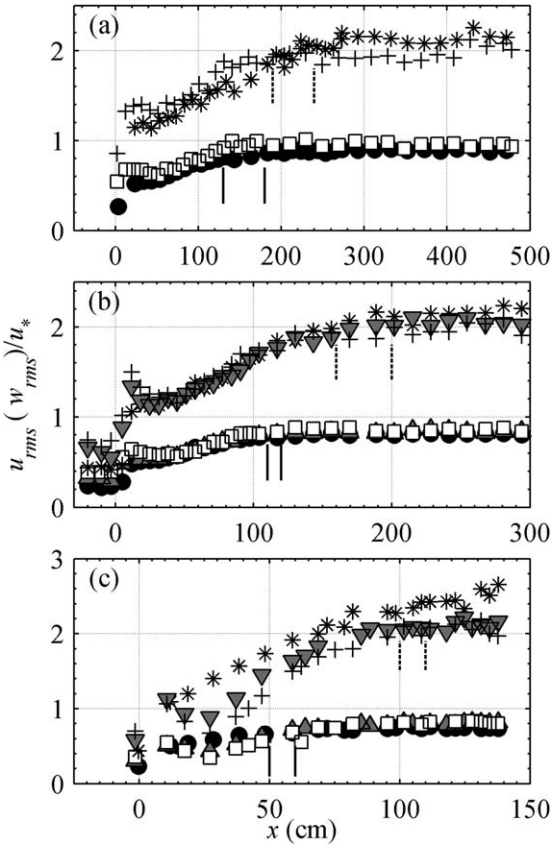

Figure 12. Turbulent rms velocity (u_{rms} and w_{rms}) at the top of the canopy ($z = h$) normalized by u_* versus distance (x) from the leading edge. (a) $a = 2.3$ m^{-1}; (b) $a = 5.1$ m^{-1}; (c) $a = 19.4$ m^{-1}. The symbols for u_{rms} are: (asterisks) $H = 14$ cm; (solid inverted triangles) $H = 22$ cm; (plus) $H = 28$ cm. The symbols for w_{rms} are: (filled circles) $H = 14$ cm; (solid triangles) $H = 22$ cm; (open squares) $H = 28$ cm. The vertical solid and dashed lines correspond to the positions for X_D and X_*, respectively.

arises purely from continuity, it should hold for any aquatic system.

[36] Finally, we consider the dependence of X_* on u_*, which reflects the efficiency with which the vortices mix vertically ($D_z \sim u_* L_s$). In our water channel u_* decreases as H/h increases (Table 1), which would tend to increase X_* with increasing H/h. However, this dependency is not strong enough to reverse the influence of $\overline{U} = f(H/h)$ described above. Further, the dependence of u_* on H/h is complicated by potentially conflicting changes in water surface slope (S), which are site specific. In our experiments, the depth-averaged velocity is held constant between cases of different water depth. As H/h decreases, the relative roughness of the canopy increases, requiring a greater water slope (S) to drive the same mean velocity, and so u_* $\left(= \sqrt{gS(H-h)}\right)$ increases, even though H-h decreases. In the field, however, changes in the velocity and water depth are often positively correlated, i.e., high flow depths are associated with high velocity, so that u_* increases with increasing H/h, which would reinforce the inverse dependency of X_* $\left(\sim \overline{U} L_s/u_*\right)$ on H/h.

[37] The evolution of the mixing-layer coherent structures is further revealed through the turbulent rms velocities measured at the top of the canopy (Figure 12). The magnitude of w_{rms} is a measure of vortex velocity. The magnitude of u_{rms} reflects the magnitude of the shear and the vertical scale of the coherent structures. First, note that the normalized values of both u_{rms} and w_{rms} have little sensitivity to flow depth. This is consistent with the fact that $H/h \geq 2$ in all cases, because previous studies (discussed above) have shown that for $H/h \geq 2$ the water surface does not constrain the evolution of the mixing layer. Second, note that w_{rms} develops over a shorter distance than u_{rms}, i.e., reaching its final, constant value closer to the leading edge, which is consistent with observations and modeling over terrestrial canopies [e.g., *Yang et al*., 2006]. The development length for w_{rms} is similar to the initial adjustment length (X_D), which is shown in the graphs for reference (Figure 12). This suggests that the strength of the coherent structures is set within this zone. This makes sense, because the velocity difference between the canopy and overflow that drives the vortex velocity is largely determined by the diminishment of U_1, which occurs over distance X_D. In contrast, the length scale for development of u_{rms} is closer to X_*, also shown in Figure 12. This makes sense if the magnitude of u_{rms} depends on the vortex scale, L_s, which develops over length X_* (Figure 9). The difference in evolution length scales between w_{rms} and u_{rms} suggests that the coherent structures reach a fixed rotational speed (w_{rms}), before they reach a final vertical scale.

[38] After the mixing layer is fully developed ($x > X_*$), the magnitude of both w_{rms} and u_{rms} at the top of the canopy scale with u_*, with no dependence on canopy density. Specifically, $w_{rms}/u_* = 0.84 \pm 0.07$ [standard deviation (SD)] and $u_{rms}/u_* = 2.1 \pm 0.14$ (SD). Similar values were measured at the top of a forest (*Morse et al*. [2002], $w_{rms}/u_* = 0.9$, $u_{rms}/u_* = 1.8$) and were reported in *Ghisalberti* [2009], who summarized data from a wide range of obstructed shear flows, finding $w_{rms}/u_* = 1.09 \pm 0.02$ [95% confidence interval (CI)], and $u_{rms}/u_* = 1.85 \pm 0.15$ (95% CI).

[39] Quadrant analysis can be used to illustrate the change in turbulence structure associated with mixing layer evolution. The instantaneous Reynolds stress $u'w'$ is divided into four quadrants [e.g., *Lu and Willmarth*, 1973].

[40] Quadrant 1: Outward interaction ($u' > 0$, $w' > 0$);

[41] Quadrant 2: Ejection ($u' < 0$, $w' > 0$);

[42] Quadrant 3: Inward interaction ($u' < 0$, $w' < 0$);

[43] Quadrant 4: Sweep ($u' > 0$, $w' < 0$);

[44] A threshold value M is used to progressively highlight (with increasing M) more extreme events within the record, i.e., only events with $|u'w'| > M|\overline{u'w'}|$ are counted. $M = 0$ means all data are considered. To isolate extreme events we choose $M = 3$, similar to *Poggi et al*. [2004b]. The ratio $S_{4,2} = \sum u'w'_{M,4} / \sum u'w'_{M,2}$ is used to quantify the relative importance of sweeps (Q4) to ejections (Q2). Here, $\sum u'w'_{M,4}$ and $\sum u'w'_{M,2}$ are the summation of instantaneous stress events which meet the threshold, $|u'w'| > M|\overline{u'w'}|$, in the fourth (sweep) and second (ejection) quadrants, respectively. Ejections dominate ($S_{4,2} < 1$) above the canopy, and sweeps dominate ($S_{4,2} > 1$) within the canopy (Figure 13). This is consistent with observations above and within terrestrial canopies [e.g., *Raupach et al*.,

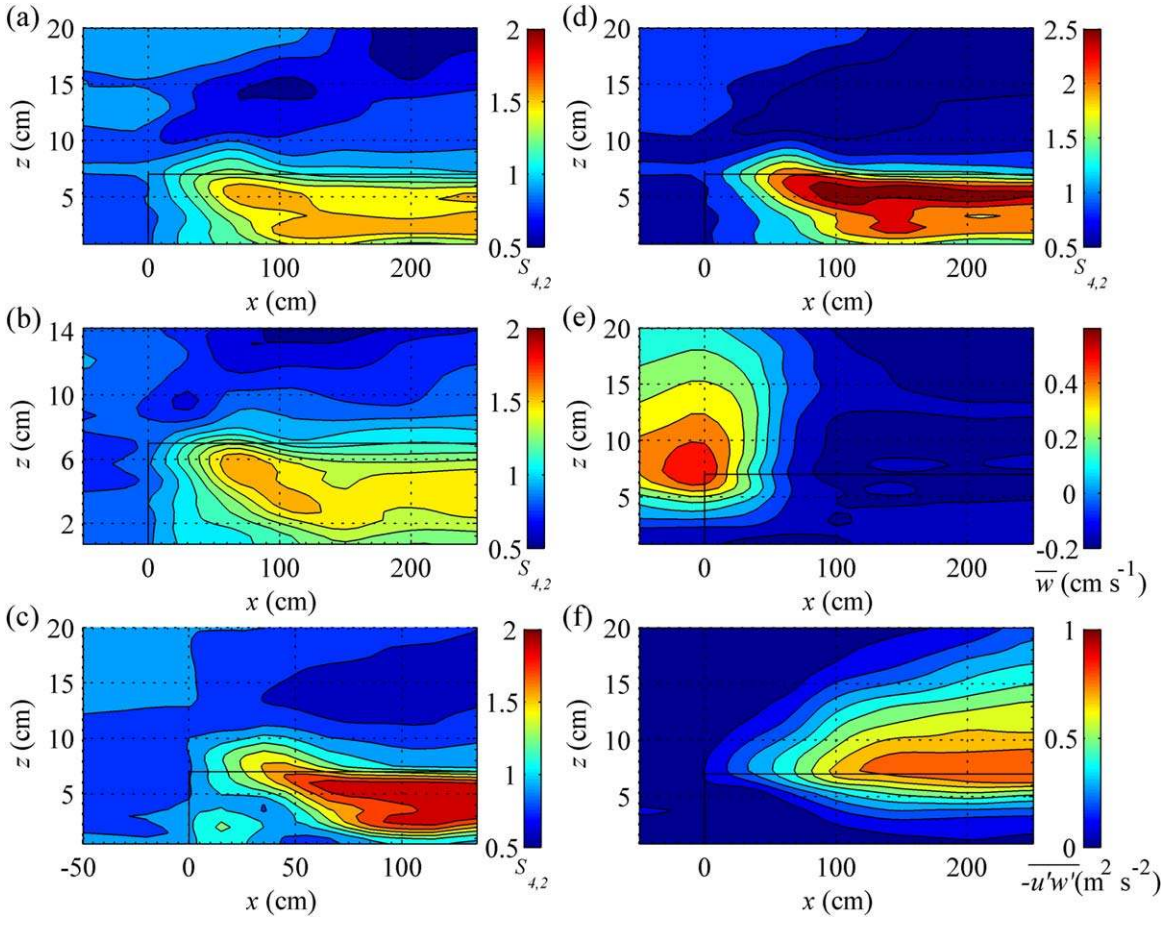

Figure 13. Subplots (a)–(d) show the ratio of sweeps to ejections, $S_{4,2}$ for cases (Figure 13a) A5 ($a = 5.1$ m^{-1}, $H/h \approx 4$) with $M = 0$; (Figure 13b) A4 ($a = 5.1$ m^{-1}, $H/h \approx 3$) with $M = 0$; (Figure 13c) A8 ($a = 19.4$m^{-1}, $H/h \approx 4$) with $M = 0$; and (Figure 13d) A5 with $M = 3$. (e) Vertical velocity for A5. (f) Reynolds stress $-\overline{u'w'}$ for A5. The canopy boundaries are shown with thin black lines at $z = 7$ cm starting at $x = 0$ cm. The figures do not extend to the water surface.

1996], and dense, submerged canopies ($ah > 0.1$, *Poggi et al*. [2004b]), but it is in contrast to boundary layer flow (e.g., upstream of the canopy), for which ejections dominate to the bed, $S_{4,2} < 1$ [*Keirsbulck et al*., 2002]. The dominance of sweeps is a key feature of canopy flow, for canopies of sufficient density. However, within sparse canopies ($ah < 0.06$), the dominance reverses, $S_{4,2} < 1$, as the flow behavior approaches that of a boundary layer [*Poggi et al*., 2004b, Figure 4]. For $ah > 0.06$, as the canopy density increases, the magnitude of $S_{4,2}(> 1)$ in the canopy increases. *Poggi et al*. [2004b] considered canopy density up to $ah = 0.5$, and for all cases they observed sweep penetration to the bed. In contrast, we consider a higher density ($ah = 1.4$, case A8, Figure 13c), for which the sweeps do not penetrate to the bed. The trends with canopy density are illustrated by comparing case A5 (Figure. 13a, $a = 5.1$ m^{-1}, $ah = 0.36$) to case A8 (Figure 13c, $a = 19.4$ m^{-1}, $ah = 1.4$). Specifically, the denser canopy (A8) experienced higher magnitudes of $S_{4,2}$ (maximum of 2.1), but the sweep events did not penetrate to the bed ($S_{4,2} < 1$ at the bed). The sparser canopy (A5) experienced smaller magnitudes in $S_{4,2}$ (maximum of 1.7), but $S_{4,2}$ remains greater than 1 (sweep dominated) over the entire canopy. Changes in water depth did not significantly alter the sweep-ejection dynamics, e.g., compare Figure 13a (A5, $a = 5.1$ m^{-1}, $H/h = 4$) to Figure 13b (A4, $a = 5.1$ m^{-1}, $H/h = 3$). The lack of dependence on H/h is expected, since we have only considered depth ratios $H/h \geq 2$, as discussed above.

[45] Finally, increasing the threshold value (M) isolates the largest events. For $M = 3$ (Figure 13d) $S_{4,2}$ is both larger within the canopy (reaching a maximum value of 2.8) and smaller above the canopy (minimum value of 0.3) than it is when all event are considered ($M = 0$, Figure 13a). This indicates that the extreme events favor sweeps within the canopy and ejections above the canopy to a greater degree than the average event. The shift from sweep to ejection dominated conditions at the top of the canopy is consistent with a mixing layer, for which sweeps dominate on the low-velocity side and ejections on the high-velocity side [e.g., *Raupach et al*., 1996].

[46] Starting from the leading edge of the canopy, the onset of sweep dominance within the canopy (a shift from blue to green to red shades) is observed only after the region of strong vertical velocity (e.g., compare Figures 13d and 13e for A5, $a = 5.1$ m^{-1}). The transition occurs first near the top of the canopy, and penetrates downward

into the canopy as the mixing layer grows. For example, for $a = 5.1\ \mathrm{m}^{-1}$ (Figures 13a, 13c, and 13e), $S_{4,2} > 1$ is first observed at $x = 30$ cm and the sweeps penetrate to their maximum depth between $x = 100$ and 140 cm. For the densest canopy (A8, $a = 19.4\ \mathrm{m}^{-1}$, Figure 13c) the adjustment begins ($S_{4,2} > 1$) at $x = 10$ cm and the sweeps penetrate to their maximum depth near $x = 70$ cm. As expected, the contour map of Reynolds stress is similar to that for $S_{4,2}$ (e.g., compare Figures 13d and 13f, A5, $a = 5.1\ \mathrm{cm}^{-1}$). However, the Reynolds stress more clearly reveals the following features. First, the Reynolds stress at the top of the canopy increases from the leading edge, but eventually reaches a constant value, which marks the fully development mixing layer. For A5, this occurs at $x = X_* = 160$ cm (Figure 13f). However, even after the mixing layer is fully developed, the shear above the canopy continues to develop. This is evident by the continued change in Reynolds stress profiles above the canopy. This progression shows distinctly that the establishment of the mixing layer occurs over a shorter distance than the establishment of the full velocity profile, which includes the boundary layer above the canopy.

6. Two Layer Model: Evolution From the Leading Edge

[47] Several researchers have suggested two-layer models for fully developed flow over a submerged canopy [e.g., *Murphy et al*., 2007; *Huthoff et al*., 2007; *Konings et al*., 2012; *Luhar and Nepf*, 2013]. In these models the flow is separated into a canopy layer ($0 \le z < h$) with vertically uniform velocity U_1 and the overflow layer ($h < z \le H$) with vertically uniform velocity U_2 (Figure 1). The layers are connected through the turbulent stress at the top of the canopy, $\tau_h = -\rho\overline{u'w'}|_{z=h}$ which has been parameterized using aspects of the vortex structure within the mixing layer [e.g., *Huthoff et al*., 2007; *Konings et al*., 2012]. Both u' and w' are expected to scale on the velocity difference between the layers ($U_2 - U_1$), so that

$$\tau_h = \rho C (U_2 - U_1)^2. \tag{13}$$

[48] The coefficient C describes the efficiency of momentum exchange between the two layers, and it should depend on the scale of the vortices at the top of the canopy. *Konings et al*. [2012] suggests that the relevant vortex scale is the penetration length scale, δ_e, defined by *Nepf et al*. [2007], which is the distance the mixing-layer vortices penetrate into the canopy, measured from the top of the canopy. This length scale is defined by the point at which the Reynolds stress within the canopy decays to a value 10% of its value at the top of the canopy [*Nepf and Vivoni*, 2000]. Like the vortex scale (L_s, discussed above) the penetration length scale also depends on both the canopy density and water depth. Specifically, δ_e is reduced when the vortex is constrained by water depth, which occurs for $H/h < 2$ [*Nepf and Vivoni*, 2000]. For $H/h > 2$, $\delta_e = 0.23(C_D a)^{-1}$ [*Nepf et al*., 2007]. For $H/h < 2$, we assume that δ_e decreases linearly to zero at $H/h = 1$, which is the emergent condition. Therefore, δ_e can be written,

$$\delta_e = \frac{0.23}{C_D a} \qquad H/h \ge 2 \tag{14}$$

$$\delta_e = \frac{0.23}{C_D a}\left(\frac{H}{h} - 1\right) \qquad H/h < 2. \tag{15}$$

[49] Using scaling arguments from *Gioia and Bombardelli* [2002], both *Huthoff et al*. [2007] and *Konings et al*. [2012] suggest the following form for the coefficient C in equation (13),

$$C = K_c\left(\frac{\delta_e}{H}\right)^{1/3} \tag{16}$$

where K_c is an empirical factor. Substituting (16) into (13), we can get

$$\tau_h = \rho K_c\left(\frac{\delta_e}{H}\right)^{1/3}(U_2 - U_1)^2. \tag{17}$$

[50] Some previous experimental data [*Murphy et al*., 2007; *Ghisalberti and Nepf*, 2004; *Poggi et al*., 2004b; *Nepf and Vivoni*, 2000; *Dunn et al*., 1996] and our own experimental data have been used to fit (17) and quantify the factor K_c. For $C_D ah < 0.2$, penetration depth calculated from (14) is larger than h, and these cases are excluded. Based on reported values of U_1, U_2, a, C_D and τ_h for each case, the best fit from (17) is $K_c = 0.07 \pm 0.02$ (SD).

[51] Using the relation for stress developed above, we can now write the continuity and layer-averaged momentum equations in the fully developed region.

[52] Continuity equation:

$$U_1 h(1 - \phi) + U_2(H - h) = U_\infty H \tag{18}$$

[53] Overflow layer momentum equation:

$$\rho g(H - h)\frac{\partial H}{\partial x} = \rho C(U_2 - U_1)^2 \tag{19}$$

[54] Canopy layer momentum equation:

$$\rho g h\frac{\partial H}{\partial x} = \frac{1}{2(1-\phi)}\rho C_D a h {U_1}^2 - \rho C(U_2 - U_1)^2 \tag{20}$$

[55] Combining (18) to (20), we solve for the canopy-layer velocity, U_1, in the fully developed region ($x > X_*$).

$$\frac{U_1}{U_\infty} = \frac{1}{1 - \frac{h}{H}\phi + \sqrt{\frac{C_D a h}{2C(1-\phi)}\left(\frac{H-h}{H}\right)^3}} \tag{21}$$

[56] Next, we extend this model to describe the evolution from the leading edge. As described earlier, velocity inside the canopy decays exponentially. Using (21) to define the final, velocity in the canopy layer (U_1), the evolution of the canopy-average velocity (U_c) from the leading edge can be described as

$$U_c(x) = U_1 + (U_0 - U_1)exp(-x/X_w) \tag{22}$$

U_0 is the canopy-averaged velocity at the leading edge ($x = 0$). The prediction of U_0 as a function of ah and H/h is

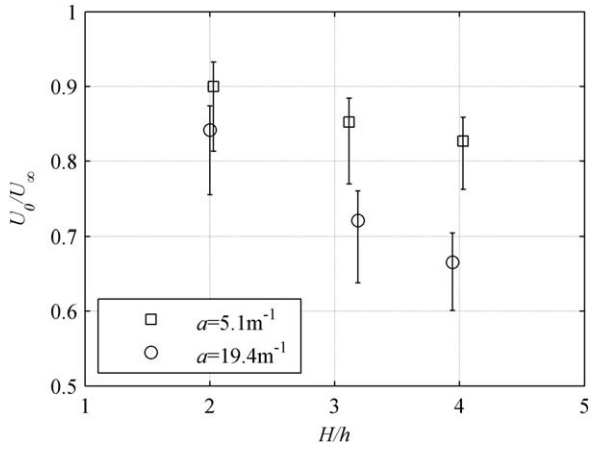

Figure 14. Relation between canopy-averaged velocity at the leading edge (U_o) and canopy density a and depth ratio H/h.

beyond the scope of this paper, and we simply use the measured U_0 (Figure 14).

[57] Equation (22) does a reasonable job describing the initial deceleration and the final velocity (Figure 15). However, it does not capture the minimum in velocity observed near 110 cm in upper figure and near 60 cm in the lower figure. This minimum occurs at the end of the initial adjustment region ($x = X_D$), and it arises because the impact of drag, which decelerates the flow, occurs over a different length scale (X_D) than the development of the shear (X_*), which accelerates the flow. That is, the increase in Reynolds stress beyond the initial adjustment ($x > X_D$) causes flow reacceleration. A reacceleration after a local minimum was also observed near the leading edge of emergent but finite width canopies, as discussed in *Rominger and Nepf* [2011].

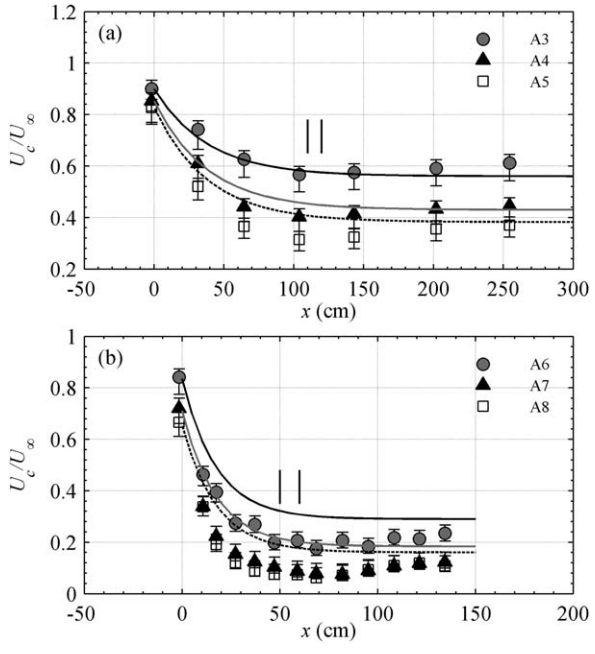

Figure 15. Measured depth-averaged velocity in the canopy layer (U_c) for (a) $a = 5.1$ m^{-1}, and (b) $a = 19.4$ m^{-1}. The solid line, gray line and dotted line correspond to predicted U_c for A3, A4, A5, and A6, A7, A8, respectively. The two short vertical lines indicate the highest and lowest value of X_D.

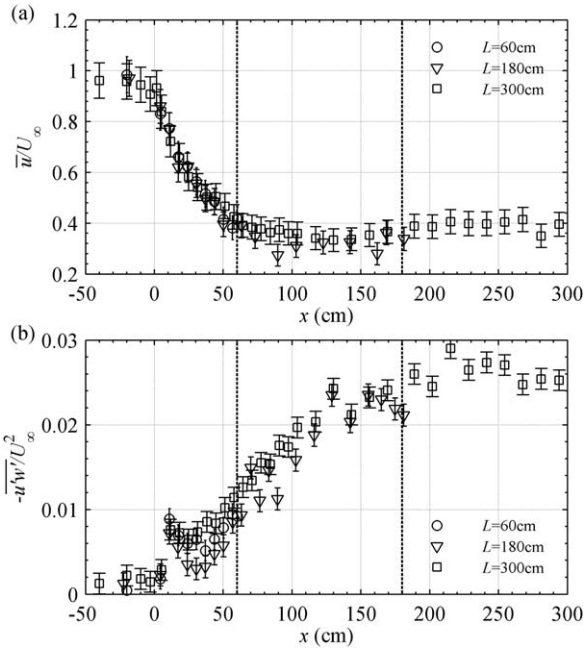

Figure 16. Streamwise velocity at midheight in the canopy and Reynolds stress at the top of the canopy for B1, B2, and B3. For all cases $a = 5.1$ m^{-1}, $H/h \approx 3$, and $X_* = 180$ cm is expected, based on B3. For B1 and B2 the canopy length $L < X_*$. The vertical dashed lines indicate the end of these two canopies.

[58] For the densest canopies, $a = 19.4$ m^{-1}, (22) overestimates the measured canopy layer velocity, U_1 (Figure 15b). This likely occurs because the assumed drag coefficient is too small. Recall that the drag coefficient $C_D = 1.6$ is estimated from the Reynolds number at the leading edge, i.e., $Re_d = U_0 d/\nu \approx 300$. However, for this dense canopy, the velocity decreases to $U_1 << U_0$, so that the local Re_d also decreases along the canopy, and in this range of Re_d, C_D increases with decreasing Re_d. If we estimate C_D based on U_1, then $C_D = 2.4$ and the predicted U_1/U_∞ would be 0.24, 0.16, and 0.14, respectively, which have better agreement with the measured values (Figure 15b). Therefore, to correct for the under estimation of C_D (and over estimation of U_1), we would need to implement an iterative solution between U_1 and $C_D = f(U_1 d/\nu)$.

[59] So far we have only considered canopies with length (L) long enough for U_1 to reach the fully developed regime ($L > X_*$). However, in the field, the canopy length L may be less than that needed to reach the fully developed in-canopy flow ($L < X_*$). We conducted additional experiments to examine the impact of canopy length on flow adjustment for the canopy density $a = 5.1$ m^{-1} and water depth $H/h = 3$, for which $X^* = 1.8$ m (Figure 16, and B1–B3; Table 1). For canopy lengths $L = 60$ cm (circle), 180 cm (inverted triangle) and 300 cm (cross), the measured velocity (Figure 16a) collapses onto the same line,

within uncertainty, indicating that the initial adjustment (X_D) is the same for all three canopy lengths. The Reynolds stresses also collapse within uncertainty (Figure 16b), which implies that the mixing layer develops similarly along all three canopies. These results suggest that canopy length is not an important factor in flow adjustment, and (22) can be used for canopies that never reach a fully developed state (i.e., $L < X_*$), even though the end condition (U_1) within (22) is defined for fully developed conditions.

7. Conclusions

[60] Flow adjustment at the leading edge of a submerged canopy was investigated using ADV and PIV measurements. The rapid flow deceleration at the leading edge can be described by a balance of flow inertia, canopy drag, and pressure, from which we show that the length of the initial adjustment scales with the nondimensional canopy drag, i.e., $X_D \sim C_D ah$. The region $x < X_D$ is marked by strong vertical advection out of the canopy, a necessary complement to the strong deceleration in streamwise velocity. The development of the mixing layer occurs over a length $X_* > X_D$. The adjustment length for the mixing layer scales with $\overline{U}L_s/u_*$, which leads to dependencies on both canopy density ($X_* \sim a^{-1}$) and depth ratio ($X_* \sim (H/h)^{-1}$). Quadrant analysis reveals the transition from ejection-dominated flow upstream of the canopy to sweep-dominated flow within the canopy. As the scale of the coherent vortices (L_s) grows from the leading edge, the sweeps penetrate further into the canopy, and reach a final, maximum penetration at distance X_*. Finally, a two-box model is used to predict the evolution of the velocity in the canopy and overflow, and measurements suggest that the canopy length (L) does not impact flow adjustment near the leading edge, i.e., the velocity within canopies shorter than X_* can be predicted from the fully developed flow equations.

[61] **Acknowledgments.** This material is based upon work supported by the National Science Foundation under grant AGS-1005480. Any opinions, findings, or recommendations expressed in this material are those of the authors and do not necessarily reflect the views of the National Science Foundation. Zhengbing Chen and Chunbo Jiang gratefully acknowledge the support of China Scholarship Council and National Natural Science Foundation of China (51279082).

References

Belcher, S., N. Jerram, and J. Hunt (2003), Adjustment of a turbulent boundary layer to a canopy of roughness elements, *J. Fluid Mech.*, *488*(1), 369–398, doi:10.1017/S0022112003005019.

Belcher, S. E., I. N. Harman, and J. J. Finnigan (2012), The wind in the willows: Flows in forest canopies in complex terrain, *Annu. Rev. Fluid Mech.*, *44*, 479–504, doi:10.1146/annurev-fluid-120710-101036.

Boström, C., E. L. Jackson, and C. A. Simenstad (2006), Seagrass landscapes and their effects on associated fauna: A review, *Estuarine Coastal Shelf Sci.*, *68*(3), 383–403, doi:10.1016/j.ecss.2006.01.026.

Brunet, Y., J. J. Finnigan, and M. R. Raupach (1994), A wind tunnel study of air flow in waving wheat: Single-point velocity statistics, *Boundary Layer Meteorol.*, *70*(1), 95–132, doi:10.1007/BF00712525.

Bunn, S. E., and A. H. Arthington (2002), Basic principles and ecological consequences of altered flow regimes for aquatic biodiversity, *Environ. Manage.*, *30*(4), 492–507, doi:10.1007/s00267-002-2737-0.

Chen, Z., A. Ortiz, L. Zong, and H. Nepf (2012), The wake structure behind a porous obstruction and its implications for deposition near a finite patch of emergent vegetation, *Water Resour. Res.*, *48*, W09517, doi:10.1029/2012WR012224.

Coceal, O., and S. Belcher (2004), A canopy model of mean winds through urban areas, *Q. J. R. Meteorol. Soc.*, *130*(599), 1349–1372, doi:10.1256/qj.03.40.

Detto, M., G. G. Katul, M. Siqueira, J. Y. Juang, and P. Stoy (2008), The structure of turbulence near a tall forest edge: The backward-facing step flow analogy revisited, *Ecol. Appl.*, *18*(6), 1420–1435, doi:10.1890/06–0920.1.

Dimotakis, P. E., F. D. Debussy, and M. M. Koochesfahani (1981), Particle streak velocity field measurements in a two-dimensional mixing layer, *Phys. Fluids*, *24*(6), 995–999, doi:10.1063/1.863481.

Dunn, C. J., F. López, and M. H. García (1996), *Mean flow and turbulence in a laboratory channel with simulated vegetation*, Hydraul. Eng. Ser. 51, Dep. of Civ. Eng., Univ. of Ill. at Urbana-Champaign, Urbana, IL.

Dupont, S., and Y. Brunet (2009), Coherent structures in canopy edge flow: A large-eddy simulation study, *J. Fluid Mech.*, *630*, 93–128, doi:10.1017/S0022112009006739.

Dupont, S., J. -M. Bonnefond, M. R. Irvine, E. Lamaud, and Y. Brunet (2011), Long-distance edge effects in a pine forest with a deep and sparse trunk space: In situ and numerical experiments, *Agric. For. Meteorol.*, *151*(3), 328–344, doi:10.1016/j.agrformet.2010.11.007.

Finnigan, J. (2000), Turbulence in plant canopies, *Annu. Rev. Fluid Mech.*, *32*(1), 519–571, doi:10.1146/annurev.fluid.32.1.519.

Folkard, A. M. (2005), Hydrodynamics of model Posidonia oceanica patches in shallow water, *Limnol. Oceanogr.*, *50*(5), 1592–1600, doi:10.4319/lo.2005.50.5.1592.

Fonseca, M. S., and M. Koehl (2006), Flow in seagrass canopies: The influence of patch width, *Estuarine Coastal Shelf Sci.*, *67*(1), 1–9, doi:10.1016/j.ecss.2005.09.018.

Gambi, M. C., A. R. M. Nowell, and P. A. Jumars (1990), Flume observations on flow dynamics in Zostera marina(eelgrass) beds, *Mar. Ecol. Prog. Ser.*, *61*(1), 159–169, doi:10.3354/meps061159.

Ghisalberti, M. (2009), Obstructed shear flows: Similarities across systems and scales, *J. Fluid Mech.*, *641*, 51–61, doi:10.1017/S0022112009992175.

Ghisalberti, M., and H. M. Nepf (2002), Mixing layers and coherent structures in vegetated aquatic flows, *J. Geophys. Res.*, *107*(C2), 3011, doi:10.1029/2001JC000871.

Ghisalberti, M., and H. M. Nepf (2004), The limited growth of vegetated shear layers, *Water Resour. Res.*, *40*, W07502, doi:10.1029/2003WR002776.

Ghisalberti, M., and H. Nepf (2005), Mass transport in vegetated shear flows, *Environ. Fluid Mech.*, *5*(6), 527–551, doi:10.1007/s10652-005-0419-1.

Ghisalberti, M., and H. M. Nepf (2009), Shallow flows over a permeable medium: The hydrodynamics of submerged aquatic canopies, *Transp. Porous Media*, *78*(2), 309–326, doi:10.1007/s11242-009-9434-x.

Gioia, G., and F. A. Bombardelli (2002), Scaling and similarity in rough channel flows, *Phys. Rev. Lett.*, *88*(1), 014501, doi:10.1103/PhysRevLett.88.014501.

Goring, D. G., and V. I. Nikora (2002), Despiking acoustic Doppler velocimeter data, *J. Hydraul. Eng.*, *128*(1), 117–126, doi:10.1061/(ASCE)0733–9429(2002)128:1(117).

Huthoff, F., D. C. M. Augustijn, and S. Hulscher (2007), Analytical solution of the depth-averaged flow velocity in case of submerged rigid cylindrical vegetation, *Water Resour. Res.*, *43*, W06413, doi:10.1029/2006WR005625.

Irvine, M., B. Gardiner, and M. Hill (1997), The evolution of turbulence across a forest edge, *Boundary Layer Meteorol.*, *84*(3), 467–496, doi:10.1023/A:1000453031036.

Keirsbulck, L., L. Labraga, A. Mazouz, and C. Tournier (2002), Surface roughness effects on turbulent boundary layer structures, *J. Fluids Eng.*, *124*(1), 127–135, doi:10.1115/1.1445141.

Konings, A. G., G. G. Katul, and S. E. Thompson (2012), A phenomenological model for the flow resistance over submerged vegetation, *Water Resour. Res.*, *48*, W02522, doi:10.1029/2011WR011000.

Kregting, L. T., C. L. Stevens, C. D. Cornelisen, C. A. Pilditch, and C. L. Hurd (2011), Effects of a small-bladed macroalgal canopy on benthic boundary layer dynamics: Implications for nutrient transport, *Aquat. Biol.*, *14*, 41–56, doi:10.3354/ab00369.

Lacy, J. R., and S. Wyllie-Echeverria (2011), The influence of current speed and vegetation density on flow structure in two macrotidal eelgrass canopies, *Limnol. Oceanogr. Fluids Environ.*, *1*, 38–55, doi:10.1215/21573698-1152489.

Lee, A. (2000), Air motion within and above forest vegetation in non-ideal conditions, *For. Ecol. Manage.,135*, *3-18*, doi:10.1016/S0378–1127(00)00294-2.

López, F., and M. García (1998), Open-channel flow through simulated vegetation: Suspended sediment transport modeling, *Water Resour. Res.*, *34*(9), 2341–2352, doi:10.1029/98WR01922.

López, F., and M. H. García (2001), Mean flow and turbulence structure of open-channel flow through non-emergent vegetation, *J. Hydraul. Eng.*, *127*(5), 392–402, doi:10.1061/(ASCE)0733-9429(2001)127:5(392).

Lu, S., and W. Willmarth (1973), Measurements of the structure of the Reynolds stress in a turbulent boundary layer, *J. Fluid Mech.*, *60*(3), 481–511, doi:10.1017/S0022112073000315.

Luhar, M., and H. M. Nepf (2013), From the blade scale to the reach scale: A characterization of aquatic vegetative drag, *Adv. Water Resour.*, *51*, 305–316, doi:10.1016/j.advwatres.2012.02.002.

Madsen, J. D., P. A. Chambers, W. F. James, E. W. Koch, and D. F. Westlake (2001), The interaction between water movement, sediment dynamics and submersed macrophytes, *Hydrobiologia*, *444*(1), 71–84, doi:10.1023/A:1017520800568.

Morris, E. P., G. Peralta, F. G. Brun, L. Van Duren, T. J. Bouma, and J. L. Perez-Llorens (2008), Interaction between hydrodynamics and seagrass canopy structure: Spatially explicit effects on ammonium uptake rates, *Limnol. Oceanogr.*, *53*(4), 1531–1539, doi:10.4319/lo.2008.53.4.1531.

Morse, A., B. Gardiner, and B. Marshall (2002), Mechanisms controlling turbulence development across a forest edge, *Boundary Layer Meteorol.*, *103*(2), 227–251, doi:10.1023/A:1014507727784.

Murphy, E., M. Ghisalberti, and H. Nepf (2007), Model and laboratory study of dispersion in flows with submerged vegetation, *Water Resour. Res.*, *43*, W05438, doi:10.1029/2006WR005229.

Nepf, H. M. (2012), Flow and transport in regions with aquatic vegetation, *Annu. Rev. Fluid Mech.*, *44*(1), 123–142, doi:10.1146/annurev-fluid-120710-101048.

Nepf, H. M., and E. R. Vivoni (2000), Flow structure in depth-limited, vegetated flow, *J. Geophys. Res.*, *105*(C12), 28,547–28,557, doi:10.1029/2000JC900145.

Nepf, H., M. Ghisalberti, B. White, and E. Murphy (2007), Retention time and dispersion associated with submerged aquatic canopies, *Water Resour. Res.*, *43*, W04422, doi:10.1029/2006WR005362.

Nezu, I., and M. Sanjou (2008), Turburence structure and coherent motion in vegetated canopy open-channel flows, *J. Hydro-environ. Res.*, *2*(2), 62–90, doi:10.1016/j.jher.2008.05.003.

Nikora, V. (2010), Hydrodynamics of aquatic ecosystems: An interface between ecology, biomechanics and environmental fluid mechanics, *River Res. Appl.*, *26*(4), 367–384, doi:10.1002/rra.1291.

Nikora, V., I. McEwan, S. McLean, S. Coleman, D. Pokrajac, and R. Walters (2007), Double-averaging concept for rough-bed open-channel and overland flows: Theoretical background, *J. Hydraul. Eng.*, *133*(8), 873–883, doi:10.1061/(ASCE)0733-9429(2007)133:8(873).

Okamoto, T., I. Nezu, and A. Katayama (2012), Developing process of large-scale coherent structure in open-channel flows with submerged vegetation, paper presented at 9th International Symposium on Ecohydraulics, IAHR-Ecohydraulics Section, Vienna, Austria.

Poggi, D., G. G. Katul, and J. D. Albertson (2004a), A note on the contribution of dispersive fluxes to momentum transfer within canopies, *Boundary Layer Meteorol.*, *111*(3), 615–621, doi:10.1023/B:BOUN.0000016563.76874.47.

Poggi, D., A. Porporato, L. Ridolfi, J. D. Albertson, and G. G. Katul (2004b), The effect of vegetation density on canopy sub-layer turbulence, *Boundary Layer Meteorol.*, *111*(3), 565–587, doi:10.1023/B:BOUN.0000016576.05621.73.

Poindexter, C. M., P. J. Rusello, and E. A. Variano (2011), Acoustic Doppler velocimeter-induced acoustic streaming and its implications for measurement, *Exp. Fluids*, *50*(5), 1429–1442, doi:10.1007/s00348-010-1001-2.

Pope, S. B. (2000), *Turbulent Flows*, Cambridge Univ. Press, Cambridge, U. K.

Raupach, M. R., J. J. Finnigan, and Y. Brunei (1996), Coherent eddies and turbulence in vegetation canopies: The mixing-layer analogy, *Boundary Layer Meteorol.*, *78*(3), 351–382, doi:10.1007/BF00120941.

Rominger, J. T., and H. M. Nepf (2011), Flow adjustment and interior flow associated with a rectangular porous obstruction, *J. Fluid Mech.*, *680*(1), 636–659, doi:10.1017/jfm.2011.199.

Sand-Jensen, K., and T. V. Madsen (1992), Patch dynamics of the stream macrophyte, Callitriche cophocarpa, *Freshwater Biol.*, *27*(2), 277–282, doi:10.1111/j.1365–2427.1992.tb00539.x.

Sukhodolov, A., and T. Sukhodolova (2006), Evolution of mixing layers in turbulent flow over submersed vegetation: Field experiments and measurement study, in *River Flow 2006: Proceedings of the International Conference on Fluvial Hydraulics*, edited by R. M. L. Ferreira et al., pp. 525–534, Taylor and Francis, Lisbon.

Sukhodolova, T. A., and A. N. Sukhodolov (2012), Vegetated mixing layer around a finite-size patch of submerged plants: 1. Theory and field experiments, *Water Resour. Res.*, *48*, W10533, doi:10.1029/2011WR011804.

Tanino, Y., and H. M. Nepf (2008), Laboratory investigation of mean drag in a random array of rigid, emergent cylinders, *J. Hydraul. Eng.*, *134*(1), 34–41, doi:10.1061/(ASCE)0733-9429(2008)134:1(34).

White, B. L., and H. M. Nepf (2007), Shear instability and coherent structures in shallow flow adjacent to a porous layer, *J. Fluid Mech.*, *593*, 1–32, doi:10.1017/S0022112007008415.

White, F. M. (1991), *Viscous Fluid Flow*, McGraw-Hill, New York.

Wilson, C., T. Stoesser, P. Bates, and A. Pinzen (2003), Open channel flow through different forms of submerged flexible vegetation, *J. Hydraul. Eng.*, *129*, 847–853, doi:10.1061/(ASCE)0733-9429(2003)129:11(847).

Wilson, N. R., and R. H. Shaw (1977), A higher order closure model for canopy flow, *J. Appl. Meteorol.*, *16*, 1197–1205, doi:10.1175/1520-0450(1977)016<1197:AHOCMF>2.0.CO;2.

Yang, B., M. R. Raupach, R. H. Shaw, K. T. P. U., and A. P. Morse (2006), Large-eddy simulation of turbulent flow across a forest edge. Part I: Flow statistics, *Boundary Layer Meteorol.*, *120*(3), 377–412, doi:10.1007/s10546-006-9057-5.

Zong, L., and H. M. Nepf (2010), Flow and deposition in and around a finite patch of vegetation, *Geomorphology*, *116*(3), 363–372, doi:10.1016/j.geomorph.2009.11.020.